Chinese Chemical Letters 31 (2020) 2774–2778

Contents lists available at ScienceDirect

Chinese Chemical Letters

journal homepage: www.elsevier.com/locate/cclet

Communication

Z-scheme heterojunction of SnS_2-decorated 3DOM-$SrTiO_3$ for selectively photocatalytic CO_2 reduction into CH_4

Wenjie He[a,b], Xingxing Wu[a], Yifei Li[a,b], Jing Xiong[a,b], Zhiling Tang[a,b], Yuechang Wei[a,b,*], Zhen Zhao[a], Xiao Zhang[a], Jian Liu[a]

[a] State Key Laboratory of Heavy Oil Processing, China University of Petroleum, Beijing 102249, China
[b] Key Laboratory of Optical Detection Technology for Oil and Gas, China University of Petroleum, Beijing 102249, China

ARTICLE INFO

Article history:
Received 11 May 2020
Received in revised form 22 June 2020
Accepted 8 July 2020
Available online 9 July 2020

Keywords:
3DOM-$SrTiO_3$
SnS_2
Z-scheme heterojunction
CO_2 conversion
CH_4 selectivity

ABSTRACT

The rapid recombination of photoinduced electron-hole pairs as well as the deficiency of high-energy carriers restricted the redox ability and products selectivity. Herein, the heterojunction of SnS_2-decorated three-dimensional ordered macropores (3DOM)-$SrTiO_3$ catalysts were *in-situ* constructed to provide transmit channel for high-energy electron transmission. The suitable band edges of SnS_2 and $SrTiO_3$ contribute to the Z-scheme transfer of photogenerated carrier. The 3DOM structure of $SrTiO_3$-based catalyst possesses the slow light effect for enhancing light adsorption efficiency, and the surface alkalis strontium is benefit to the boosting adsorption for CO_2. The in-situ introduced SnS_2 decorated on the macroporous wall surface of 3DOM-$SrTiO_3$ altered the primary product from CO to CH_4. The Z-scheme electron transfer from SnS_2 combining with the holes in $SrTiO_3$ occurred under full spectrum photoexcitation, which improved the excitation and utilization of photogenerated electrons for CO_2 multi-electrons reduction. As a result, $(SnS_2)_3$/3DOM-$SrTiO_3$ catalyst exhibits higher activity for photocatalytic CO_2 reduction to CH_4 compared with single SnS_2 or 3DOM-$SrTiO_3$, *i.e.*, its yield and selectivity of CH_4 are 12.5 $\mu mol\ g^{-1}\ h^{-1}$ and 74.9%, respectively. The present work proposed the theoretical foundation of Z-scheme heterojunction construction for enhancing photocatalytic activity and selectivity for CO_2 conversion.

The shortage of fossil energy resources and the global climate warming is threatening the living environment of human beings. The photocatalysis technology for carbon dioxide (CO_2) reduction to sustainable hydrocarbon energy may perfectly addresses the above conundrums [1–8]. However, the artificial photosynthesis technique is faced with the low solar energy conversion efficiency as well as the rare products [9–12]. Thus, it is significant to develop high performance photocatalyst. The perovskite-type $SrTiO_3$ possesses the wide band gap whose conduction band is positive enough to reduce CO_2, hence it was been widely researched for photoreduction reaction [13–19]. In addition, CO_2 as the anhydride of carbonic acid is more likely to adsorb with alkalis strontium on the surface of $SrTiO_3$ [20–22], so that it is promising to further investigate. However, the wide band gap of $SrTiO_3$ plays a double-edged sword, which can not only decrease the recombination of electron-hole pairs, but also restrains the visible light absorption and the photoexcitation. Thus, the pristine $SrTiO_3$ is faced with the low quantum utilization and less multi-electron products [23,24]. The strategies should be proposed to optimize $SrTiO_3$ and construct a novel catalyst with outstanding photoreduction performance as well as multi-electrons product (CH_4) selectivity.

Three-dimensional ordered macroporous (3DOM) catalysts as photonic crystals have been extensively studied in the field of photocatalysis due to their slow light efficiency [25–31]. Photonic crystals have periodic refractive modulation in the optical wavelength range, which can cause stopband reflection through the Bragg diffraction of the material and prohibit light propagation at certain wavelengths. The contact time between the photon and the material was extended, and the incident light of a specific wavelength is stored in 3DOM materials, thus the light capturing efficiency could be improved. And 3DOM structure could be obtained by replicating a classic face-centered cubic opal structure template [32–34]. In addition, tin disulfide (SnS_2), whose band gap is about 1.9–2.4 eV, is one of the most important layered transition metal sulfides [35–37]. The unique atomic arrangement in SnS_2,

* Corresponding author at: State Key Laboratory of Heavy Oil Processing, China University of Petroleum, Beijing 102249, China.
E-mail address: weiyc@cup.edu.cn (Y. Wei).

https://doi.org/10.1016/j.cclet.2020.07.019
1001-8417/

two layers of S atoms in the middle of two Sn atomic layers formed a built-in electric field perpendicular to the (001) crystal plane, is help to promote the directional migration of electrons [38–42]. And SnS_2 as the n-type semiconductor was used to investigate the adjustment of electrons structure in photocatalytic system.

Herein, SnS_2 nanosheets were *in-situ* constructed on the surface of 3DOM-$SrTiO_3$, and novel SnS_2/3DOM-$SrTiO_3$ catalysts with Z-scheme heterojunction were obtained. SnS_2 can absorb the full spectrum light and plays a role of electrons contributor. The photogenerated electrons achieved Z-scheme transmission affected by built-in electric field between layers *via* the hybrid interface [43–45]. SnS_2/3DOM-$SrTiO_3$ catalysts exhibited high the activity for CO_2 photoreduction and altered the predominant products selectivity from CO to CH_4 under full spectrum light irradiation in comparison to 3DOM-$SrTiO_3$. Thus, the present work will propose a way for increasing multi-electrons reduction process and reach to the high yield of the multi-electron products of CO_2 photoreduction.

The 3DOM-$SrTiO_3$ was synthesized by colloidal crystal template (CCT) method and SnS_2 was induced by co-hydrothermal as shown in Scheme S1 (Supporting information). The $(SnS_2)_n$/3DOM-$SrTiO_3$ catalysts were obtained and the specific amount of reagent nd corresponding products are listed in Table S1 (Supporting information). For clarification of the prepared catalysts, Fig. 1 exhibits scanning electron microscopy (SEM) images of the catalysts. SnS_2 shows regular hexagonal nanosheet structure with diameter of ~200 nm in Fig. S1a (Supporting information). As shown in Figs. 1b and c, the catalysts exhibit the ordered 3D network structure connected by the porous windows, and SnS_2 nanosheets distribute to the ordered channels of 3DOM-$SrTiO_3$. The compact arrangement structure benefits to the photoinduced electrons transfer between SnS_2 and 3DOM-$SrTiO_3$, and the relatively high specific surface area provides the abundant sites for CO_2 adsorption and photoreduction in Table S2 (Supporting information). The X-ray diffraction (XRD) patterns were exhibited in Fig. S1 (Supporting information). The diffraction peaks of $(SnS_2)_n$/3DOM-$SrTiO_3$ catalysts perfectly matched with Hexagonal phase SnS_2 (JCPDS No. 23-0677) and Cubic phase $SrTiO_3$ (JCPDS No. 35−0734), respectively.

Furthermore, the phase structures of SnS_2 and $(SnS_2)_3$/3DOM-$SrTiO_3$ catalysts were further analyzed by Raman spectroscopy using an excitation wavelength of 532 nm (Fig. S2 in Supporting information). The Raman spectrum of SnS_2 exhibits a strong band at 314 cm^{-1}, which corresponds to the A_{1g} vibration mode of SnS_2. Moreover, a weak vibration peak at 205 cm^{-1} is shown in the inset of Fig. S2, it is attributed to the E_g vibration mode of SnS_2. Meanwhile, the strong Raman bands of $(SnS_2)_3$/3DOM-$SrTiO_3$ catalyst located at 145, 397, 517 and 638 cm^{-1} are attributed to the Raman-active transverse optical phonons of TO_2, TO_3, TO_4 and longitudinal optical phonons of LO_4 of $SrTiO_3$, respectively. In addition, the A_{1g} vibration peak of SnS_2 detected at 314 cm^{-1}. It demonstrates that the original chemical bond structure of the catalyst $SrTiO_3$ support is not affected by the composite SnS_2 nanosheets, and the appearance of the A_{1g} vibration peak of SnS_2 also indicates that it is tight contact with $SrTiO_3$, resulting in heterojunction structure.

The light absorption property of the catalysts is precondition of well photocatalytic activity, the photoexcitation efficiency of charge separation depends on the light absorption efficiency. As shown in Fig. S3a (Supporting information), after SnS_2 nanosheets constructed on 3DOM-$SrTiO_3$, the optical absorption bands of $(SnS_2)_n$/3DOM-$SrTiO_3$ catalysts have red-shift compared with pristine $SrTiO_3$, indicating that the light absorption is enhanced in the visible region (from 400 nm to 800 nm). The photoluminescence (PL) spectra of the catalysts were used to provide evidences for further understand the photoinduced charge carrier migration and separation efficiency. Fig. 2 shows the PL spectrum of $(SnS_2)_n$/3DOM-$SrTiO_3$ catalysts excited at an wavelength of 390 nm. Obviously, there is one PL emission peaks of pristine SnS_2 located at 520 nm. It attributes to the recombination of electron-hole pairs on the surface or inner of SnS_2 nanosheets. However, 3DOM-$SrTiO_3$ catalyst has not PL emission peak, indicating the low recombination. $(SnS_2)_n$/3DOM-$SrTiO_3$ catalysts possess one PL emission peaks near to 520 nm, furthermore, the intensity of emission peak decreases with increasing of the SnS_2 dosage, suggesting that the rapidly transfer of photoexcited electrons under irradiation could be suppressed. For the reason that the E_{CB} and E_{VB} of SnS_2 are between E_{CB} and E_{VB} of $SrTiO_3$, if carriers transfer through heterojunction Type I path, they will rapidly recombine and fail to effective separation. So that electrons were located on $SrTiO_3$ while the holes on SnS_2 after separation and Z-scheme transmission. It is attributed to the Z-scheme heterojunction role of $(SnS_2)_n$/3DOM-$SrTiO_3$ catalysts. It is noticed that, when SnS_2 composite content is increased to 5%, the intensity of emission peak belongs to $(SnS_2)_5$/3DOM-$SrTiO_3$ is enhanced. It indicates that the suitable dosage of SnS_2 contributes to the charge transfer, and the excess SnS_2 leads to the formation of

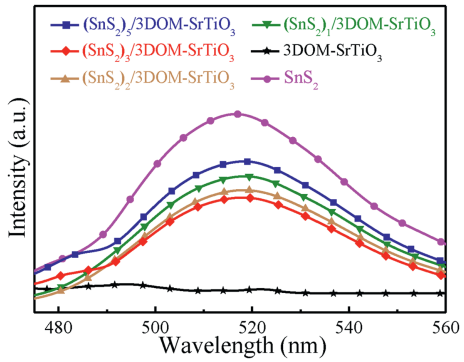

Fig. 2. The photoluminescence spectra of SnS_2, 3DOM-$SrTiO_3$ and $(SnS_2)_n$/3DOM-$SrTiO_3$ catalysts.

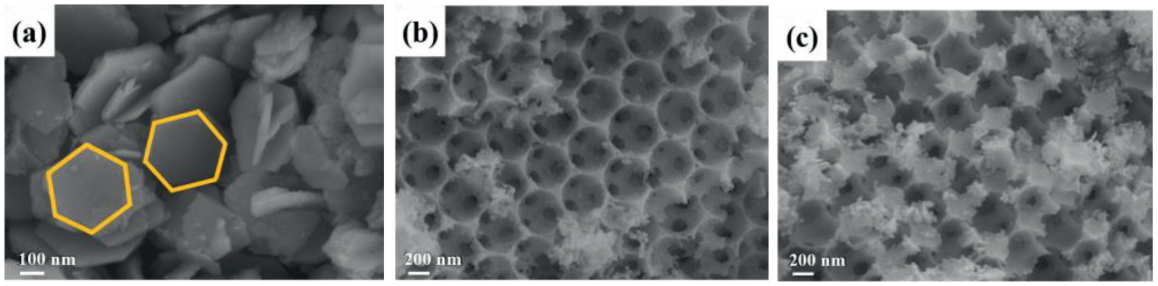

Fig. 1. SEM images of SnS_2 (a), 3DOM-$SrTiO_3$ (b) and $(SnS_2)_3$/3DOM-$SrTiO_3$ (c) catalysts.

recombination center, hence the photogenerated electron-hole pairs recombination efficiency increased.

Photocatalytic CO_2 reduction tests were conducted to evaluate the activity of the catalysts. The carbon-containing organic compounds of CO and CH_4 as the predominant reduction products were detected, and their curves of output over time are shown in Figs. 3a and b, respectively. All the catalysts possess the activity for CO_2 photoreduction as well as clean-energy production under the accordant conditions. 3DOM-$SrTiO_3$ catalyst exhibits the largest formation rates of CO product, while $(SnS_2)_3$/3DOM-$SrTiO_3$ catalyst has the largest formation rates of CH_4 product. Actually, there are two reactions (CO_2 reduction and H_2O oxidation) in the whole photocatalysis system. The two reduction reactions require to consume photogenerated electrons. Hence, the photocatalytic reduction of H_2O to H_2 occurs as a competitive reaction to the CO_2 photocatalytic reduction. In detail, 3DOM-$SrTiO_3$ catalyst exhibits the higher selectivity (90.4%) for CO_2 photoreduction in comparison with P25 (67.2%) and SnS_2 (71.2%) shown in Fig. 3c. It contributes to the three-dimensional ordered macropores structure in favor of CO_2 adsorption. Both P25 and 3DOM-$SrTiO_3$ catalysts have the higher CO selectivity (Fig. 3d), which are 61.1% and 58.9%, respectively. It is attributed to the wide band gap limited the electron-hole pairs separation and hindered the multi-electrons reduction process. In contrary, the pristine SnS_2 catalyst possesses the narrow band gap performance with slightly higher CH_4 selectivity (51.4%). After introduction of SnS_2 nanosheets with narrow band gap, it is noted that the yield of CH_4 product is enhanced while CO product is decreased (Fig. 3d). It suggests that the SnS_2 nanosheets are able to act as electrons supplier, providing enough electrons for CO_2 reduction as well as CH_4 production. With the increasing dosage of SnS_2, the activity of $(SnS_2)_n$/3DOM-$SrTiO_3$ photocatalysts present a volcano variation trend. As shown in Table S3 (Supporting information), the yield of CH_4 over $(SnS_2)_n$/3DOM-$SrTiO_3$ catalysts reached to the highest amount about 12.5 $\mu mol\,g^{-1}\,h^{-1}$ when the SnS_2 dosage is 3.0%. In addition, $(SnS_2)_3$/3DOM-$SrTiO_3$ catalyst also exhibits the best CO_2 reduction property (91.4%) as well as CH_4 selectivity (74.9%). The significant improvement of CH_4 product selectivity can be affected by the binary compounds, indicating that SnS_2 nanosheets play a key role to provide electrons in this photocatalytic CO_2 reduction system. It is noteworthy that the binary catalysts consisted of the SnS_2 and 3DOM-$SrTiO_3$ inherited the preeminent CO_2 photoreduction selectivity from 3DOM-$SrTiO_3$. The formed Z-scheme heterojunction effectively increased the photogenerated electrons and greatly facilitates the enhancing selectivity and yield of CH_4 product. The photocatalytic activity for CO_2 reduction decreased with further increasing the amount of SnS_2, indicating that the proportion of SnS_2 in 3DOM-$SrTiO_3$ is also crucial, the excess SnS_2 possesses negative effect to the photocatalytic reaction, which is attributed to the direct recombination of photogenerated electron-hole pairs in the SnS_2 nanosheets for decreasing photocatalytic performance of CO_2 conversion. Although SnS_2 can absorb the ultraviolet and visible light, the rapid recombination of photogenerated electron-hole pairs limited its performance for CO_2 photoreduction. It is consistent with the results of UV–vis and PL spectra. In addition, the half reaction of H_2O oxidation to O_2 caused by valence band of semiconductor is also significant. Therefore, the produced protons participate in the hydrogenation reactions for the formation of hydrocarbons.

To understand the process of charge separation as well as CO_2 photoreduction in this binary system, the pathway of electrons transmission and reactant conversion were proposed. As describes above, the energy gap (E_g) values of $SrTiO_3$ and SnS_2 are 2.94 eV and 1.76 eV, respectively (Fig. S3b in Supporting information). As shown in Fig. 4, the conduction band potential (E_{CB}) of $SrTiO_3$ (−1.36 V *vs.* NHE at pH 7) [46] and SnS_2 (−0.56 V *vs.* NHE at pH 7) [47] is more negative than the reduction potentials of CO_2 to CH_4 (−0.24 V) and CO_2 to CO (−0.53 V), hence both $SrTiO_3$ and SnS_2 could reduce CO_2 to CH_4 and CO in theory, which is consistent with the results of CO_2 photoreduction. Moreover, the adsorption capacity of CO_2 was enhanced by constructing the three-dimensional ordered macropores structure in the present work.

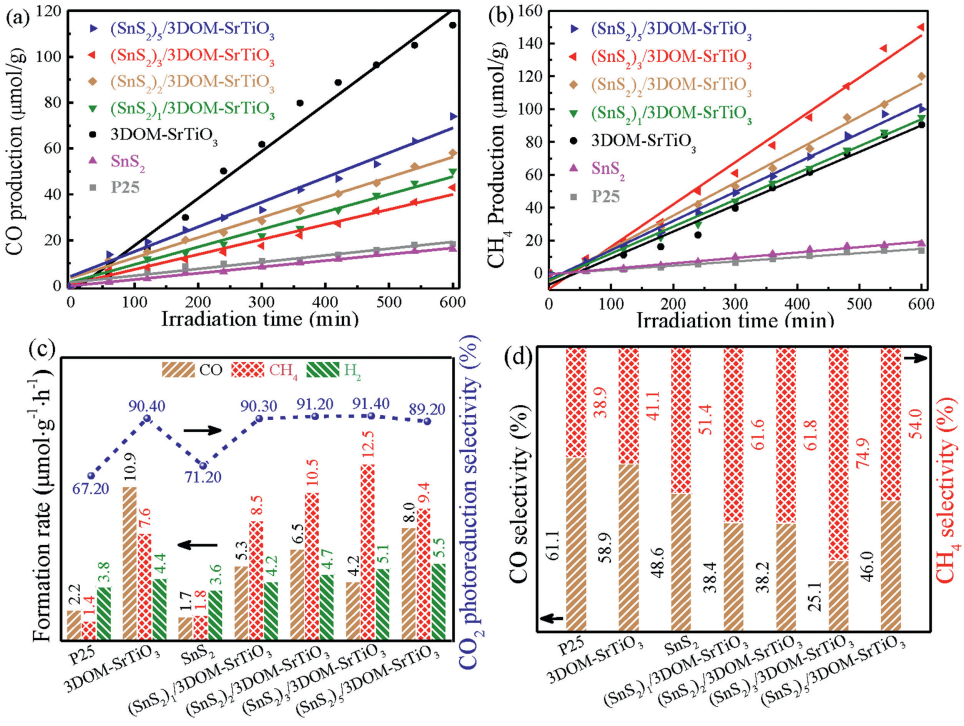

Fig. 3. CO (a) and CH_4 (b) products over SnS_2, 3DOM-$SrTiO_3$ and $(SnS_2)_n$/3DOM-$SrTiO_3$ catalysts. (c) CO_2 photoreduction selectivity as well as the products formation rate of CO, CH_4 and H_2. (d) The CO and CH_4 selectivity.

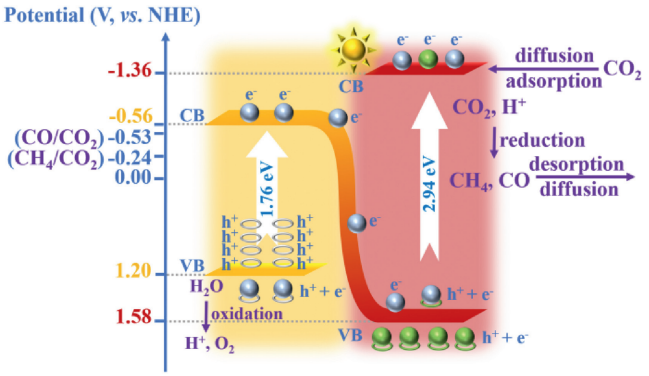

Fig. 4. Schematic diagram of electron-hole pairs separation and the possible reaction mechanism of SnS_2/3DOM-$SrTiO_3$ under simulative solar irradiation.

The perovskite type $SrTiO_3$ catalyst containing alkalis was employed, for the interaction built between Sr and CO_2, and which plays a significant role in the adsorption and activation of CO_2 [48]. In order to improve the photon capture efficiency, the constructed 3DOM structure with unique pores which could appear the slow light effect [49], as well as the introduced SnS_2 cocatalyst with narrow band gap is contributed to the excellent light adsorption. In addition, the separation and transfer efficiency of photogenerated carriers were enhanced by establishing Z-scheme heterojunction between $SrTiO_3$ and SnS_2.

Herein, the binary $(SnS_2)_n$/3DOM-$SrTiO_3$ catalysts exhibit higher performance for photocatalytic CO_2 reduction than the SnS_2 and 3DOM-$SrTiO_3$ catalysts. Furthermore, the exist of SnS_2 in the binary structure (SnS_2/3DOM-$SrTiO_3$) absolutely enhanced the CH_4 selectivity compared with 3DOM-$SrTiO_3$, especially altered the main selectivity from CO (S_{CO} = 58.9% over 3DOM-$SrTiO_3$) to CH_4 (S_{CH_4} = 74.9% over $(SnS_2)_3$/3DOM-$SrTiO_3$). The SnS_2 with the narrow band gap contributed to the large absorption in visible light region, resulting in the efficiency utilization of photons and more free electrons to be excited. The electrons separate with holes at the valence band of SnS_2 and transfer to the conduction band, then transmit through the interface (between SnS_2 and 3DOM-$SrTiO_3$) to the conduction band of $SrTiO_3$ which effected by the internal electric field of SnS_2. Meanwhile, $SrTiO_3$ excited by ultraviolet light and the photogenerated electrons transfer from valence band to conduction band. It demonstrates that the Z-scheme transmission of photoexcited electrons enabled the electron-hole pairs recombination decreased and enriched the high energy electrons at the conduction band of $SrTiO_3$. In addition, the alkalis strontium on the surface of $SrTiO_3$ contributes to the adsorption of CO_2, resulting in the adequate adsorption intensity for CO_2 accepting multi-electrons. Thus, the multi-electrons process of CO_2 reduction occurred, and the enhanced CH_4 selectivity due to the localization of electrons and the suitable CO_2 adsorption ability on the surface of $SrTiO_3$. The binary compounds possess the higher performance for CO_2 reduction and more multi-electrons process to form CH_4.

In summary, the present work proposed a novel binary SnS_2/3DOM-$SrTiO_3$ with Z-scheme heterojunction improved the photocatalytic carbon dioxide reduction performance. The three-dimensional ordered macropores structure of 3DOM-$SrTiO_3$ facilitated the utilization of light, and the *in situ* introduced SnS_2 with narrow band gap is benefits to the boosting absorption of visible light. The atom Sr as the alkalis in the perovskite type $SrTiO_3$ is favor the adsorption and excitation of CO_2. In addition, the Z-scheme transmission of photoexcited electrons enabled the electron-hole pairs recombination decreased and enriched the high energy electrons at the conduction band of $SrTiO_3$, resulting the higher carbon dioxide reduction performance and more multi-electrons process to form CH_4, hence the predominant products selectivity altered from CO to CH_4. The study in this binary system provides a novel *in-situ* construction method and photogenerated electrons transfer strategy, the work may shed new light on the photoreduction performance and multi-electrons process improvement.

Declaration of competing interest

The authors declare that they have no known competing financial interests or personal relationships that could have appeared to influence the work reported in this paper.

Acknowledgments

This work was supported by the National Natural Science Foundation of China (Nos. 21673142, 21972166), Beijing Natural Science Foundation (No. 2202045), PetroChina Innovation Foundation (No. 2018D-5007-0505) and Science Foundation of China University of Petroleum, Beijing (Nos. 242017QNXZ02, 2462018BJC005).

Appendix A. Supplementary data

Supplementary material related to this article can be found, in the online version, at doi:https://doi.org/10.1016/j.cclet.2020.07.019.

References

[1] Y. Yang, S. Ajmal, X. Zheng, Susrain. Energ. Fules 2 (2018) 510–537.
[2] S. Habisreutinger, L. Schmidt-Mende, J. Stolarczyk, Angew. Chem. Int. Ed. 52 (2013) 7372–7408.
[3] J.G. Ran, M. Jaroniec, S.Z. Qiao, Adv. Mater. 30 (2018) 1704649.
[4] A. Tjandra, J. Huang, Chin. Chem. Lett. 29 (2018) 734–746.
[5] C. Dong, J. Ji, Z. Yang, et al., Chin. Chem. Lett. 30 (2019) 853–862.
[6] L. Hao, L. Kang, H.W. Huang, et al., Adv, Mater. 31 (2019) 1900546.
[7] X. Chang, T. Wang, J. Gong, Energ. Environ. Sci. 9 (2016) 2177–2196.
[8] L. Qiao, M. Song, A. Geng, et al., Chin. Chem. Lett. 30 (2019) 1273–1276.
[9] C. Wang, Y. Zhao, H. Xu, et al., Appl. Catal. B 263 (2020) 118314.
[10] F. Wang, X. Yu, M. Ge, et al., Chem. Eng. J. 384 (2020) 123381.
[11] S. George, S. Pokhrel, Z. Ji, et al., J. Am. Chem. Soc. 133 (2011) 11270–11278.
[12] T. Inoue, A. Fujishima, S. Konishi, et al., Nature 277 (1979) 637–638.
[13] H.J. Yoon, M.S.K. Kim, W.X. Huang, et al., Chin. Chem. Lett. 29 (2018) 800–804.
[14] J. Shan, F. Raziq, M. Humayun, et al., Appl. Catal. B 219 (2017) 10–17.
[15] K. Shao, Y. Wang, M. Iqbal, et al., Appl. Surf. Sci. 434 (2018) 717–724.
[16] C. Luo, J. Zhao, Y. Li, et al., Appl. Surf. Sci. 447 (2018) 627–635.
[17] Q. Kang, T. Wang, P. Li, et al., Angew. Chem. Int. Ed. 54 (2015) 841–845.
[18] S. Shoji, A. Yamaguchi, E. Sakai, et al., ACS Appl. Mater. Interfaces 9 (2017) 20613–20619.
[19] T. Townsend, N. Browning, F. Osterloh, ACS Nano 6 (2012) 7420–7426.
[20] J. Lan, D.P. Cao, W.C. Wang, et al., ACS Nano 4 (2010) 4225–4237.
[21] X. Meng, S. Ouyang, T. Kako, et al., Chem. Commun. 50 (2014) 11517–11519.
[22] Q. Tang, Z. Sun, P. Wang, et al., Appl. Surf. Sci. 463 (2019) 456–462.
[23] S. Shoji, G. Yin, M. Nishikawa, et al., Chem. Phys. Lett. 658 (2016) 309–314.
[24] B. Kumar, J. Smieja, C. Kubiak, J. Phys. Chem. C 114 (2010) 14220–14223.
[25] S. Xie, J. Deng, S. Zang, J. Catal. 322 (2015) 38–48.
[26] J. Liang, Y. Zheng, J. Chen, et al., Angew. Chem. Int. Ed. 51 (2012) 3892–3896.
[27] M. Zalfani, B. Schueren, M. Mahdouani, et al., Appl. Catal. B 199 (2016) 187–198.
[28] Y. Chang, K. Yu, C.X. Zhang, et al., Appl. Catal. B 215 (2017) 74–84.
[29] J. Liu, H. Zhao, M. Wu, et al., Adv. Mater. 29 (2017) 1605349.
[30] Y. Lu, H. Yu, S. Chen, et al., Environ. Sci. Technol. 46 (2012) 1724–1730.
[31] L. Sun, M. Yang, J. Huang, et al., Adv. Funct. Mater. 26 (2016) 4943–4950.
[32] Q. Wu, M. Jing, Y. Wei, et al., Appl. Catal. B: Environ. 244 (2019) 628–640.
[33] L. Tang, Z. Zhao, Y.C. Wei, et al., Catal. Today 297 (2017) 131–142.
[34] Y. Wei, J. Liu, Z. Zhao, et al., Energ. Environ. Sci. 4 (2011) 2959–2970.
[35] Y. Zhang, Z. Du, K. Li, et al., ACS. Appl. Mater. Interfaces 3 (2011) 1528–1537.
[36] Z. Zhang, J. Huang, M. Zhang, et al., Appl. Catal. B 163 (2015) 298–305.
[37] J. Yu, C. Xu, F. Ma, et al., ACS. Appl. Mater. Interfaces 6 (2014) 22370–22377.
[38] S. Chen, J. Wang, J. Huang, et al., Chin. J. Chem. Phys. 30 (2017) 36–42.
[39] J. Liu, E. Hua, J. Phys, Chem. C 121 (2017) 25827–25835.
[40] Y. Wang, Y. Tian, Z. Lang, et al., J. Mater. Chem. A 6 (2018) 21056–21063.
[41] Y. Ma, X. Zhao, M. Niu, et al., RSC Adv. 7 (2017) 25582–25588.
[42] H.M. Huang, B.Y. Dai, W. Wang, et al., Nano Lett. 17 (2017) 3803–3808.
[43] Y. Li, K. Lv, W. Ho, et al., Int. J. Appl. Catal. B 202 (2017) 611–619.

[44] W. Ouyang, F. Teng, X. Fang, Adv. Func. Mater. 28 (2018) 1707178.
[45] M. Ding, J. Zhou, H. Yang, et al., Chin. Chem. Lett. 31 (2020) 71–76.
[46] H. Tan, Z. Zhao, W. Zhu, et al., ACS Appl. Mater. Interfaces 6 (2014) 19184–19190.
[47] T. Di, B. Zhu, B. Cheng, et al., J. Catal. 352 (2017) 532–541.
[48] X. Wu, C. Wang, Y. Wei, et al., J. Catal. 377 (2019) 309–321.
[49] Y. Wei, J. Jiao, Z. Zhao, et al., Appl. Catal. B 179 (2015) 422–432.